Received: 8 December 2022 | Revised: 6 April 2023 | Accepted: 22 April 2023

DOI: 10.1002/gamm.202300010

ORIGINAL PAPER

GAMM Mitteilungen

Optimal operation of dielectric elastomer wave energy converters under harmonic and stochastic excitation

Matthias K. Hoffmann[1] | **Lennart Heib**[1] | **Giacomo Moretti**[2] | **Gianluca Rizzello**[3] | **Kathrin Flaßkamp**[1]

[1]Systems Modeling and Simulation, Saarland University, Saarbrücken, Saarland, Germany

[2]Department of Industrial Engineering, Università di Trento, Trentino Alto-Adige, Italy

[3]Adaptive Polymer Systems, Saarland University, Saarbrücken, Saarland, Germany

Correspondence
Matthias K. Hoffmann, Systems Modeling and Simulation, Saarland University, Saarbrücken, Saarland, Germany.
Email: matthias.hoffmann@uni-saarland.de

Funding information
European Union's Horizon 2020, Grant/Award Number: 893674; Italian Ministry of Education, University and Research

Abstract

Dielectric elastomers are a promising technology for wave energy harvesting. An optimal system operation can allow maximizing the extracted energy and, simultaneously, reducing wear that would lead to a reduction in the wave harvester lifetime. We pursue a model-based optimization approach to identify optimal controls for wave energy harvesters based on dielectric elastomers. First, a direct method is used for time-discretization of the dielectric elastomer wave energy harvester in the optimal control problem. The two conflicting objectives are considered in a multiobjective optimization framework. Considering a periodic, sinusoidal wave excitation, the optimal solution shows turnpike properties for the optimal periodic mode of operation. However, since real wave motion is neither monochromatic nor predictable on longer time horizons, further extensions are pursued. First, we introduce a stochastic wave excitation. Second, an iterative model-predictive control scheme is designed. Due to multiple objectives, the control scheme has to include an automated adaption of the corresponding priorities. Here, we propose and evaluate a heuristic rule-based adaption in order to maintain the damage below target levels. The approach presented here might be used in the future to guarantee for autonomous operation of farms of wave energy harvesters.

KEYWORDS

dielectric elastomers, model predictive control, multiobjective optimization, nonlinear optimization, optimal control, wave energy converters

1 | INTRODUCTION

Among the various forms of renewable energies, ocean wave energy is one of the most abundant and highly concentrated sources. However, to date high technological complexity and capital costs have prevented wave energy converter (WEC) technologies from reaching the market [24]. This motivates, first, the search for new technological solutions and, second, a systematic systems engineering approach for modeling, simulation, and optimization-based operation strategies to accurately predict the full potential of novel approaches.

Recently, dielectric elastomer generators (DEGs) have shown to be promising for providing the technological breakthrough: Being lightweight polymeric generators, they are potentially cheaper and simpler solutions than conventional power take-off systems for wave energy [22]. DEGs enable direct-drive mechanical-to-electrical power conversion based

on a variable-capacitance principle. In the last decade, numerical analyses and wave tank tests have uncovered the potential of this technology [21].

Developing numerical models of DEG-WECs opens up important opportunities towards the development of advanced controls, including: a controller design taking into account nonlinear system characteristics, an optimization-based control strategy to maximize energy harvest, as well as lifetime predictions by minimizing damage during operation. Ocean waves are irregular and therefore unpredictable on long time horizons [6]. This causes a conceptual problem for open-loop optimal control for WEC: prediction errors of the wave excitation result in derived control signals that lead to suboptimal system behavior only, that is, the predicted energy harvest cannot be reached. One way to address this issue is to consider receding horizon methods such as optimization-based model-predictive control (MPC).

1.1 | Related work

In [9], an overview on optimal control and MPC approaches for wave energy systems is given. Also, [26] addresses the control problem of DEG-WEC systems and suggests dynamic programming techniques.

Heuristic control strategies for DEG power take-off systems are based on a pre-fixed bang-bang structure [22]. To the best of the authors' knowledge, our previous work [16] was the first on multiobjective optimization of DEG-WEC systems. The energy cost function considers the effect of electrical losses within the dielectric elastomer, unlike in [26], and we include an objective for lifetime optimization. Based on a nonlinear system model, in [16], we computed Pareto-optimal trade-offs which allow for a reduction of damage by more than 50% while only losing 1% of energy compared to a control that only aims at maximizing the power. Here, excitation had been reduced to monochromatic waves and fictitiously long prediction horizons were assumed.

Work on lifetime and long-term reliability of DEG power take-off systems is still rare. In [5] the authors observed that electrical breakdown is the main cause of failure for DEGs. However, the application of large electric fields is key if large energy conversion densities are sought.

MPC can be used to overcome the need for long-term predictions of wave excitation, [9]. In [15], we give a detailed study on the MPC prediction horizon needed to obtain solutions acceptably close to the optimal control ground truth. When considering multiple objectives, decision making needs to be automated within the MPC loop. This additional degree of freedom can be used to control long-time goals such as predictable residual lifetime taking into account past system operating conditions. For wind energy harvesting, this idea is described in detail in [25]. A simple switching heuristic has been presented in [15], already.

1.2 | Contribution

Based on our two previous publications [15,16], we present an in-depth study of the excitation effects, that is, monochromatic versus stochastic waves, on the DEG-WEC device. For the monochromatic case, we observe periodic turnpikes in the optimal solution. While turnpike properties are of mathematical, analytical interest and are usually considered positive characteristics of optimal control problems, we obtain undesired behavior in our MPC implementations: due to the receding horizon but unused leaving arcs, the control amplitudes continuously shrink and, thus, the energy yield reduces in each cycle. However, these effects are of academic nature only, since a monochromatic model of wave excitation is far from being realistic. Turning to stochastic wave inputs, our numerical evaluations show that the MPC performance is unaffected by turnpike-like behavior. Lastly, we consider two different objectives and present decision making strategies for the multiobjective MPC setting. That is, the optimization of the energy harvested by the DEG in a reference time frame, and the minimization of a damage cost accounting for the DEG cyclic electrical loading are considered simultaneously.

Our approach outperforms heuristic bang-bang controllers used in literature, that is, it converts larger amounts of wave energy, even in the presence of safer lower electric fields.

1.3 | Outline

The remainder of this article is structured as follows: the model of a pitching flap WEC with dielectric elastomer generator is derived in Section 2, followed by a derivation of cost functions and problem statements for single- and

multiobjective optimal control in Section 3. In Section 4, numerical results indicate the periodic turnpike behavior of the DEG-WEC under sinusoidal excitation. Afterwards, the MPC problem is solved for stochastic wave excitation in Section 5 and the weight control heuristic is presented. Final remarks and an outlook to future work is given in Section 6.

2 | PITCHING FLAP WAVE ENERGY CONVERTER WITH DIELECTRIC ELASTOMER GENERATOR

WECs are electro-mechanical systems that harvest mechanical energy from the waves and convert them into usable electrical energy. Different WEC concepts have been proposed, which consist of a floater (e.g., a heaving buoy or an articulated multi-body floating structure [24]) acting as a primary interface that absorbs energy from the incident wave loads and transfers it to an electro-mechanical power take-off (PTO) system (e.g., an electric machine driven directly by the floater motion, or by an intermediate hydraulic ram), which is responsible for the final mechanical-to-electrical power conversion. Among PTO technologies proposed so far, a particularly promising solution is offered by DEGs, a class of elastomeric electrostatic generators, which might allow reducing the architectural complexity and cost, and improve the adaptability of WECs to the marine environment compared to traditional electromagnetic PTO systems. DEG-based WECs have been the object of several research works in the last few years, which went through the development of device concepts, mathematical models, and scaled experimental demonstrators [7,21]. These proof-of-concept analyses suggested that DEGs might become a relevant player in the wave energy market, which is worth further research. Nonetheless, the future development of DEG-WECs passes through a number of open questions, including the extent to which DEG technology can be upscaled, the maximum energy performance that can he achieved, and the durability/reliability that a DEG PTO can reach. Regarding these latter points, we remark that the ability of a DEG to convert electrical energy depends on the electric field to which it is subject (namely, its cyclic convertible energy density grows quadratically with the applied electric field [22]). Whereas large working fields are key to obtain consistent energetic performance, they are also responsible for the accumulation of electrical damage and failure in the material.

With the aim of providing methodological tools to assess the energetic performance and tendency to accumulate electrical damage of DEG-WECs, we hereby make reference to a special device layout, shown in Figure 1. The system consists of a pitching flap (or paddle), hinged to the sea bottom and put into oscillation by the waves. Whereas this system has been traditionally studied in combination with hydraulic PTO systems [29], here we consider an implementation which makes use of a parallelogram-shaped DEG, as proposed by Moretti et al. [19,20]. The parallelogram DEG (Figure 1B) consists of a stack of dielectric elastomer membranes, pre-loaded in the planar directions and attached through their perimeter to the links of a parallelogram mechanism (namely, a four-bar mechanism with couple of links with equal length). Neighbor dielectric membranes are separated by stretchable electrodes with alternated polarity, so as to form a deformable capacitor, which provides the flap with a controllable force, which can be regulated by varying the voltage applied on the electrodes.

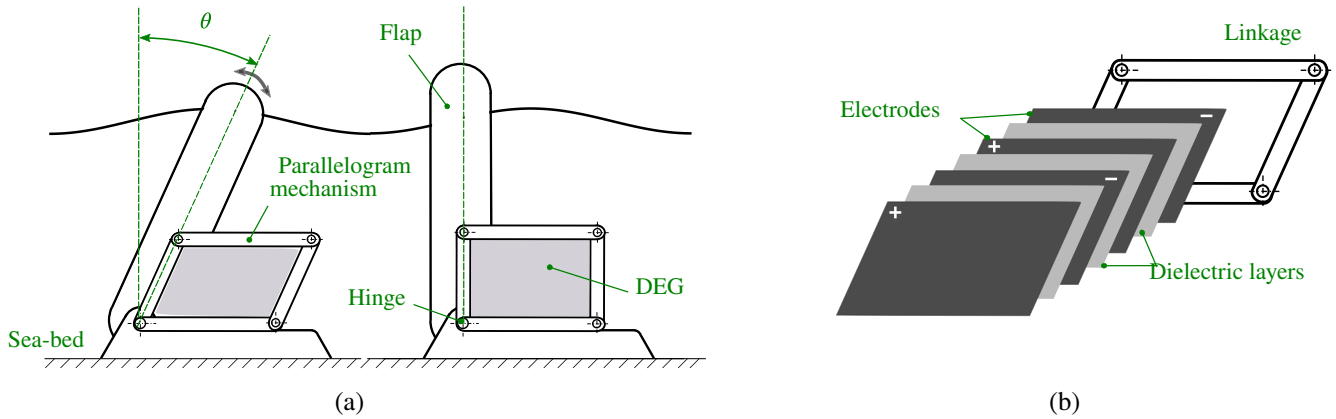

FIGURE 1 (A) Schematic of the pitching flap WEC with DEG. (B) Exploded view of the DEG PTO system, showing the multi-layer architecture of the active membrane.

Wave-induced oscillations of the flap induce a cyclic capacitance variation of the DEG. The system configuration can be uniquely identified by means of the flap pitch angle θ with the vertical axis. Assuming that the DEG membrane is equally pre-stretched in the planar directions, $\theta = 0$ is an equilibrium position for the system. The DEG surface (and, hence, its capacitance) is maximum when the flap is in the vertical position, and it decreases as $|\theta|$ increases. Cyclically controlling the applied voltage allows converting input mechanical work done by the waves on the flap into electrical energy. Heuristic control strategies used to drive DEGs so as to generate electrical energy follow a four-phase logic [22]:

- When the DEG capacitance increases (namely, in the phases where $\theta\dot{\theta} < 0$), no voltage is applied on the electrodes, and the DEG behaves as a passive elastic element.
- When the DEG reaches maximum capacitance ($\theta = 0$ crossing), the DEG is charged at a target voltage, and electrical energy is preliminary spent (priming).
- While the DEG capacitance decreases ($\theta\dot{\theta} > 0$), a voltage is applied on the electrodes. Coulomb forces between opposite-polarity electrodes [19] generate a resisting torque on the flap (opposing the flap's velocity), which extracts mechanical energy from the system and transfers it to the DEG in the form of electrical energy.
- When the capacitance value reaches a minimum, the DEG is fully discharged, and stored electrostatic energy is recovered.

Two cycles like those described above take place during a single oscillation of the flap. The maximum voltage applied on the DEG during the electrically active phases must be compatible with the static breakdown limits of the polymeric dielectrics, and the damage accumulated by the material because of the electric field.

Although this heuristic guarantees that the DEG produces a positive electrical energy gain in each oscillation, an improvement of the energy extracted from the system can be obtained by optimizing the time history of the applied voltage, leveraging on the system dynamics.

In the following, a dynamic model of the WEC is briefly summarized, based on the work previously published in [16,20]. The model is built upon the assumption that the flap pitch oscillation is small ($\theta \ll 1$ rad), and it describes the dynamics of the device in terms of equations of motion of the pitching flap coupled with the wave field (see Figure 2A). The model state equations are given as follows:

$$\begin{aligned}
\dot{x}(t) &= \begin{bmatrix} 0 & 1 & 0^{1\times n} \\ -I_h^{-1}K_\mathrm{h} & -I_\mathrm{h}^{-1}B_\mathrm{h} & -I_\mathrm{h}^{-1}C_\mathrm{r} \\ 0^{n\times 1} & B_\mathrm{r} & A_\mathrm{r} \end{bmatrix} x(t) + \begin{bmatrix} 0 \\ I_\mathrm{h}^{-1} \\ 0^{n\times 1} \end{bmatrix} \left(d(t) - \gamma x_1(t) v^2(t) \right), \\
x(t) &= \begin{bmatrix} \theta(t) & \delta(t) & z(t)^\top \end{bmatrix}^\top = \begin{bmatrix} x_1(t) & x_2(t) & x_3(t) & x_4(t) & x_5(t) \end{bmatrix}^\top, \\
x(0) &= x_0.
\end{aligned} \tag{1}$$

In (1), the inputs are given by the applied voltage $v(t) \in \mathbb{R}$ and the time wave excitation torque $d(t) \in \mathbb{R}$, while the state variables correspond to the flap angle $\theta(t) = x_1(t) \in \mathbb{R}$, the flap angular velocity $\delta(t) = x_2(t) \in \mathbb{R}$, and a state describing the dynamics of the torques due to the radiated waves generated by the flap motion, $z(t) = \begin{bmatrix} x_3(t) & x_4(t) & x_5(t) \end{bmatrix}^\top \in \mathbb{R}^3$. The model parameters are given by stiffness $K_\mathrm{h} \in \mathbb{R}$ (rendering the hydrostatic stiffness and the DEG elastic stiffness, though the latter is negligible in the considered application [20]), damping $B_\mathrm{h} \in \mathbb{R}$ (due to viscous losses in the fluid or the elastomer), inertia $I_\mathrm{h} \in \mathbb{R}$, an electrostatic coupling parameter $\gamma \in \mathbb{R}$, and matrices $A_\mathrm{r} \in \mathbb{R}^{3\times 3}$, $B_\mathrm{r} \in \mathbb{R}^{3\times 1}$, and $C_\mathrm{r}^\top \in \mathbb{R}^3$ which describe the wave radiation process. The contribution of the electrostatic forces is rendered via a term (right-hand side of (1)) that, for small oscillation angles, can be assumed proportional to v^2 and x_1. We also introduce an output for model (1), denoted as $i(t) \in \mathbb{R}$, and physically representing the current flowing in the WEC:

$$i(t) = \frac{v(t)}{R_0} + \frac{d\left(\left(C_0 - \gamma\theta^2(t)\right)v(t)\right)}{dt} = \frac{v(t)}{R_0} - 2\gamma\theta(t)\delta(t)v(t) + \left(C_0 - \gamma\theta^2(t)\right)\dot{v}(t), \tag{2}$$

where $R_0 \in \mathbb{R}$ and $C_0 \in \mathbb{R}$ define a leakage resistance and a nominal capacitance, respectively. From (2), it can be noted that the current is essentially given as the sum of two contributions, which correspond to a parallel connection between a leakage resistance R_0 and a configuration-dependent capacitance ($C_0 - \gamma\theta^2(t)$), respectively (see Figure 2B).

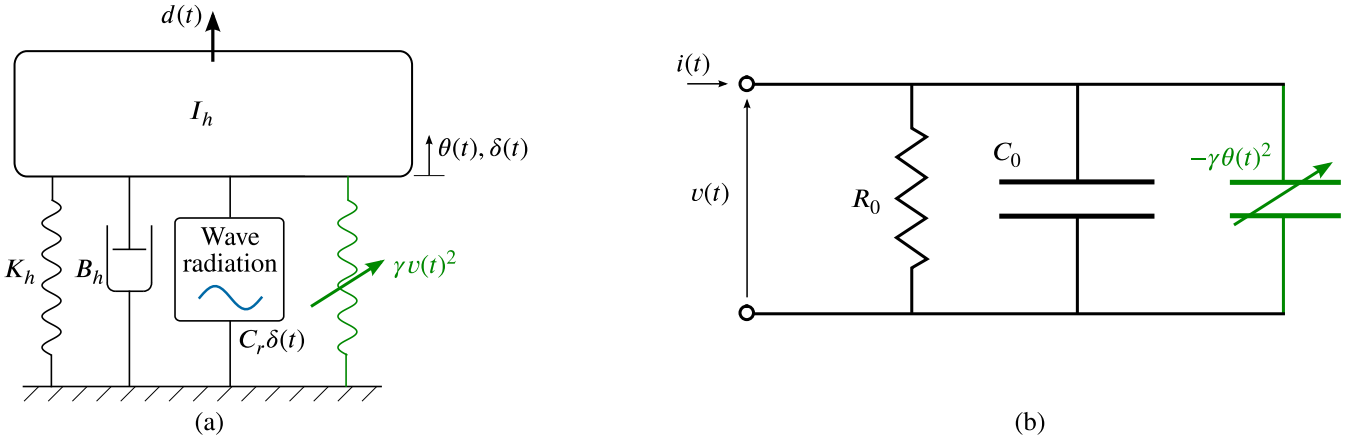

FIGURE 2 Equivalent lumped-parameter models of the flap mechanical response (A), and the DEG electrical response (B). Components in green (variable mechanical stiffness, variable capacitance) are responsible for electro-mechanical coupling effects.

Assumption 1. The input voltage is restricted within the closed set $[0,\ v_{\max}]$ for a given $v_{\max} > 0$, that is, $v(t) \in [0,\ v_{\max}]\ \forall\ t$.

Assumption 2. The parameters of model (1) are such that $K_{\mathrm{h}} > 0,\ B_{\mathrm{h}} \geq 0,\ I_{\mathrm{h}} > 0,\ C_0 > 0,\ R_0 > 0$, $K_{\mathrm{h}} - \gamma v_{\max}^2 \geq 0$, and there exist matrices $Q = Q^{\top} \in \mathbb{R}^{3\times 3}$ and $S = S^{\top} \in \mathbb{R}^{3\times 3}$ such that

$$\begin{aligned} &Q \succeq 0, \\ &QA_{\mathrm{r}} + A_{\mathrm{r}}^{\top} Q = -2S \preceq 0, \\ &QB_{\mathrm{r}} = C_{\mathrm{r}}^{\top}. \end{aligned} \tag{3}$$

Assumption 1 sets a constraint on the input, which needs to be satisfied in operative conditions. Restricting v to positive values accounts for constraints in the power electronics (e.g., the use of unipolar power converters), without implications on the controller capability (choosing a negative voltage is not meaningful since model (1) solely depends on $v^2(t)$). Upper bounding v allows for preventing static breakdown of the dielectric elastomeric material. Indicating with E_{bd} the ultimate breakdown electric field of the elastomer, and noticing that for $\theta \ll 1$ rad the electric field is equal to $e(t) = v(t)/h_{\mathrm{l}}$ (h_{l} being the initial thickness of the dielectric layers in the DEG stack), a technically meaningful estimate for $v_{\max}$ is given as follows:

$$v \leq v_{\max} = E_{\mathrm{bd}} h_{\mathrm{l}}. \tag{4}$$

Assumption 2, on the other hand, holds true for physically consistent values of the model parameters. In particular, condition (3) implies that the wave radiation model is passive, which is usually assumed to hold true [33]. Both assumptions shall hold true for a well-designed device.

It can be proved that the WEC model (1) and (2) satisfies the following structural property, which is instrumental for the optimal control result presented in the sequel.

Proposition 1. *Under Assumptions 1 and 2, model (1) is dissipative with respect to the following storage function*

$$\lambda_{\mathrm{WEC}}\ (x(t)) = \frac{1}{2} I_{\mathrm{h}} \delta^2(t) + \frac{1}{2} K_{\mathrm{h}} \theta^2(t) + \frac{1}{2} z(t)^{\top} Q z(t), \tag{5}$$

and supply rate

$$s_{\mathrm{WEC}}\ (x(t), v(t)) = \delta(t) d(t) - \gamma \delta(t) \theta(t) v^2(t). \tag{6}$$

TABLE 1 Case study parameters.

Param.	Value	Param.	Value
I_h	2.3×10^7 kg m^2	h_l	275 μm
C_h	2×10^6 N m s	E_{bd}	120 kV/mm
K_h	1.7×10^7 N m	E_{th}	80 kV/mm
C_0	139 mF	n_d	2
R_0	3.4 kΩ	α	10^{-6} kV^{-4}s^{-1}

Proof. Assumptions 1 and 2 imply that $\lambda_{\mathrm{WEC}}(x(t))$ as defined by (5) is always non-negative, thus it can be qualified as a storage function. The time derivative of (5) is computed as follows:

$$\dot{\lambda}_{\mathrm{WEC}}(x(t)) = I_{\mathrm{h}}\delta(t)\dot{\delta}(t) + K_{\mathrm{h}}\theta(t)\dot{\theta}(t) + \frac{1}{2}\dot{z}(t)^{\top}Qz(t) + \frac{1}{2}z(t)^{\top}Q\dot{z}(t). \tag{7}$$

Replacing the states time derivatives from (1) in (7), we obtain

$$\dot{\lambda}_{\mathrm{WEC}}(x(t)) = -B_{\mathrm{h}}\delta^2(t) + \frac{1}{2}z(t)^{\top}(QA_{\mathrm{r}} + A_{\mathrm{r}}^{\top}Q)z(t) + z^{\top}(t)\left(QB_{\mathrm{r}} - C_{\mathrm{r}}^{\top}\right)\delta(t) + \delta(t)d(t) - \gamma\delta(t)\theta(t)v^2(t). \tag{8}$$

By using the second and third equations in (3), we can rewrite (8) as

$$\dot{\lambda}_{\mathrm{WEC}}(x(t)) = -B_{\mathrm{h}}\delta^2(t) - z(t)^{\top}Sz(t) + \delta(t)d(t) - \gamma\delta(t)\theta(t)v^2(t) \leq \delta(t)d(t) - \gamma\delta(t)\theta(t)v^2(t) \equiv s_{\mathrm{WEC}}(x(t), v(t)), \tag{9}$$

where the inequality in (9) follows from Assumption 2. Integration of (9) in the time interval $[t_0,\ t_1]$ allows us to conclude dissipativity with respect to storage function $\lambda_{\mathrm{WEC}}(x(t))$ and supply rate $s_{\mathrm{WEC}}(x(t), v(t))$, thus concluding the proof. ∎

Remark 1. Storage function (5) and dissipativity inequality (9) can readily be interpreted from a physical point of view. In particular, the term appearing on the right-hand side of (5) corresponds to the kinetic energy stored in the flap, potential energy stored in the fluid, and an energy accumulation term due to the wave dynamics. At the same time, the contributions in the second term of (9) represent mechanical power dissipated due to viscous torques on the flap, mechanical power dissipation due to wave radiation, mechanical power supplied by the wave, and the supplied electrical power that is converted into mechanical power by the DE.

For the numerical analyses presented in the rest of the article, we refer to the parameters listed in Table 1 [16].

3 | SINGLE- AND MULTIOBJECTIVE OPTIMAL CONTROL PROBLEM

Given a dynamical control system

$$\dot{x} = f(t, x(t), u(t)), \qquad x(0) = x_0 \tag{10}$$

with state $x \in \mathbb{X} \subset \mathbb{R}^n$, initial state $x_0 \in \mathbb{X}$ and control $u \in \mathbb{U} \subset \mathbb{R}^m$, we assume that for any control signal $u : [t_0, t_1] \to \mathbb{U}$ of a suitable chosen function space and on time interval $[t_0, t_1] \subset \mathbb{R}_{\geq 0}$, there exists a unique solution $\varphi(t, u|_{[t_0,t]}, x_0) \in \mathbb{X}$ for all $t \in [t_0, t_1]$, which we briefly denote by $x : [t_0, t_1] \to \mathbb{X}$. An optimal control problem can be stated as

$$\min_{x,u} J(x, u) = \int_{t_0}^{t_1} \ell(t, x(t), u(t))\,\mathrm{d}t\ , \tag{11}$$

$$\text{s.t. } \dot{x} = f(t, x(t), u(t)), \qquad \forall t \in [t_0, t_1], \tag{12}$$

$$x(t) \in \mathbb{X},\ u(t) \in \mathbb{U} \qquad \forall t \in [t_0, t_1], \tag{13}$$

$$x(0) = x_0, \qquad r(x(T)) = 0, \tag{14}$$

where $\ell : \mathbb{R}^n \times \mathbb{R}^m \to \mathbb{R}$ denotes the running/stage costs (or Lagrange term) of the cost functional $J : \mathbb{R}^n \times \mathbb{R}^m \to \mathbb{R}$, it is typically assumed to be continuously differentiable. The system equations enter as constrains of the minimization problem. Equation (13) can be given in terms of nonlinear state- or state-control constraints, as linear constraints, in special cases, or in terms of box constraints. Also, Equation (14) gives one possible type of boundary constraint, already aiming for the problem set-up we are faced with in this article.

In our numerical studies, we apply a direct optimal control method, that is, we use the CasADi package by [2], which is linked with algorithmic differentiation for providing derivatives, and the IPOPT interior points method by [28].

In a multiobjective optimal control problem (MOCP), the aim is to minimize multiple objectives, $J_i : \mathbb{R}^n \times \mathbb{R}^m \to \mathbb{R}$, $i = 1, \dots, K$ at the same time. Since the objectives might be contradicting, the solution of an MOCP consists of the set of optimal compromises, called the Pareto set. Via direct methods, an MOCP is transcribed into a multiobjective optimization problem, for which various kinds of solution methods exist: scalarization techniques, which allow to apply classical gradient-based methods, set-oriented methods, genetic algorithms, or evolutionary strategies. For an overview see, for example, [17] and the references cited therein. Recent work studies MOCP in view of MPC solution methods, using dissipativity arguments to ensure MPC-stability in a multicriteria setting [12,14].

In this work, we use the Normal Boundary Intersection (NBI) method for scalarizing the vectorial costs and computing discrete points along the Pareto front

$$\mathcal{P} = \left\{ \begin{pmatrix} J_1(x^*, u^*) \\ J_2(x^*, u^*) \end{pmatrix} \,\middle|\, (x^*, u^*) = \arg\min_{x \in \mathbb{X}, u \in \mathbb{U}} -l \text{ w.r.t. (1) and } w_1 M_1 + w_2 M_2 + l\hat{n} \geq J(x,u)^\top \text{ for } (w_1, w_2) \in \mathbb{W} \right\},$$

where $\mathbb{W}$ is a finite set of n_w pre-chosen weights with $w_{1,i} + w_{2,i} = 1$ for $i = 1, \dots, n_\mathrm{w}$. M_i is the extreme point to the ith cost function, so

$$M_i = J(x^{*,i}, u^{*,i}), \text{ with } (x^{*,i}, u^{*,i}) = \arg\min_{x \in \mathbb{X}, u \in \mathbb{U}} J_i(x,u) \text{ w.r.t. dynamics (1)}, \tag{15}$$

the costs when only one cost function is minimized. The NBI method shoots a vector of length l from the boundary plane, the convex combination of all extreme points, in the normal direction $\hat{n}$ onto the Pareto front, where the intersection point is found as a solution of the problem.

3.1 | Cost functions for DEG-WEC optimal control

For convenience, we rewrite model (1) and (2) by applying the change of input coordinate $u(t) = v^2(t)$, thus obtaining

$$\begin{aligned} \dot{x}(t) &= \begin{bmatrix} 0 & 1 & 0^{1\times n} \\ -I_h^{-1}K_\mathrm{h} & -I_\mathrm{h}^{-1}B_\mathrm{h} & -I_\mathrm{h}^{-1}C_\mathrm{r} \\ 0^{n\times 1} & B_\mathrm{r} & A_\mathrm{r} \end{bmatrix} x(t) + \begin{bmatrix} 0 \\ I_\mathrm{h}^{-1} \\ 0^{n\times 1} \end{bmatrix} (d(t) - \gamma x_1(t) u(t)), \\ i(t) &= \frac{\sqrt{u(t)}}{R_0} - 2\gamma\theta(t)\delta(t)\sqrt{u(t)} + \left(C_0 - \gamma\theta^2(t)\right) \frac{\dot{u}(t)}{2\sqrt{u(t)}}, \end{aligned} \tag{16}$$

and $\mathbb{U} = \left\{ u \in \mathbb{R} \;\middle|\; 0 \leq u \leq v_\mathrm{max}^2 \right\}$. We can define two meaningful cost functions for (16), which correspond to technically relevant control goals.

The first one corresponds to the electric energy extracted by the WEC, which represents a quantity that has to be maximized. In the adopted convention, the instantaneous extracted power is given by the product $-i(t)v(t)$. Therefore, in order to maximize energy extraction, the following cost function has to be minimized

$$J_1(x, u, t_0, t_1) = \int_{t_0}^{t_1} i(t)\sqrt{u(t)}\, \mathrm{d}t\ . \tag{17}$$

By defining the WEC's total electro-mechanical energy as

$$\Psi(x(t),u(t)) = \lambda_{\text{WEC}}\ (x(t)) + \frac{1}{2}\left(C_0 - \gamma\theta^2(t)\right)u(t) = \frac{1}{2}I_h\delta^2(t) + \frac{1}{2}K_h\theta^2(t) + \frac{1}{2}z(t)^\top Qz(t) + \frac{1}{2}\left(C_0 - \gamma\theta^2(t)\right)u(t), \tag{18}$$

where the term proportional to $u(t)$ represents the electrostatic potential energy stored in the DEG, and exploiting (9) with $u(t) = v^2(t)$, the time derivative of (18) on the trajectories of (16) can be computed as follows

$$\dot{\Psi}(x(t),u(t)) = -B_h\delta^2(t) - z(t)^\top Sz(t) - \frac{u(t)}{R_0} + \delta(t)d(t) + i(t)\sqrt{u(t)}. \tag{19}$$

In virtue of (19), (17) can be rewritten as follows

$$J_1(x,u,t_0,t_1) = \Psi(x(t_1),u(t_1)) - \Psi(x(t_0),u(t_0)) + \int_{t_0}^{t_1}\left(B_h\delta^2(t) + z(t)^\top Sz(t) + \frac{u(t)}{R_0} - \delta(t)d(t)\right)\mathrm{d}t. \tag{20}$$

The integral terms in J_1 represent the difference between the mechanical power supplied by the waves to the flap ($\delta(t)d(t)$) and the power dissipated by the different loss sources (viscosity, waves radiation, Joule losses), whereas the term outside of the integral represents the difference in stored electro-mechanical energy between the initial and final instants.

The second cost function accounts for the damage accumulated in the DEG upon cyclic operation. Studies on the cyclic lifetime of DEGs [1,4,5] point out that the main source of damage accumulation is the presence of large applied electric fields, whose influence is far more significant than that of mechanical damage. Based on experimental evidence [8], it can be assumed that electric damage only accumulates when the electric field ($e(t) = v(t)/h_l$) is larger than a threshold value E_{th} (with $E_{\text{th}} < E_{\text{bd}}$), and a damage cost function (to be minimized through control) can be formulated as follows:

$$J_2(x,u,t_0,t_1) = \alpha\int_{t_0}^{t_1}\left(\max\{u(t) - E_{\text{th}}^2h_l^2, 0\}\right)^2\mathrm{d}t, \tag{21}$$

where α is a normalization factor which renders J_2 dimensionless. We remark that (21) is a heuristic cost, used here with the aim of capturing, in an approximated manner, a threshold damage accumulation process. Since a high electric field is necessary for good energy extraction, these two costs contradict each other, where the most efficient usage is typically found in the middle between the two extremes.

Problem 1. Combining costs (17) and (21), and using dynamic equation (1) and Assumption 1 as constraints, allows casting the following multiobjective optimal control problem

$$\begin{aligned}&\underset{u}{\text{minimize}} \quad J = [J_1, J_2]\\ &\text{s.t. dynamics (1)}\\ &0 \le \cos^2(\theta(t))\,u(t) \le (E_{\text{bd}}h_l)^2\ \forall t \in [t_0,\ t_1],\end{aligned} \tag{22}$$

where the optimal control time history, u, is to be determined.

In the following sections, we present the numerical results of Problem 1. In our implementation, direct methods for optimal control are used to calculate an approximation of u, concretely the classical Runge–Kutta method. For u and d, first-order hold behavior is assumed and all $\cos^2(\cdot)$-terms are linearized to be 1 such that the results shown are a lower bound for the performance. The optimization problem is formulated using CasADi [2] and solved with IPOPT, an interior point algorithm [28].

4 | OPTIMAL SOLUTIONS WITH PERIODIC TURNPIKE BEHAVIOR UNDER SINUSOIDAL EXCITATION

Since its introduction by Willems [30,31], dissipativity has played an important role in optimal control (OC) and (economic) MPC for proving stability [11,13,23,32]. Originally, dissipativity has been stated w.r.t. controlled steady-state

solutions. The state-control pairs, on which the average stage costs are the lowest, define a *turnpike*. Optimal solutions approach this steady-state and dwell there for as long as boundary conditions and the time horizon given within the optimal control problem (OCP) allow for [10,27].

The concept can be extended to optimally controlled systems that exhibit limit cycles. Zanon et al. [34] develop the dissipativity based on the definition of the periodic trajectory. It is given in discrete time. Thus, we assume to have transformed our Problem 1 by applying a numerical discretization scheme, for example, classical Runge–Kutta as proposed at the end of Section 3.

Definition 1 (Periodic trajectory and distance measure, see [34]). A sequence $X^P = (\bar{x}[0], \bar{x}[1], \dots)$ is called a feasible P-periodic trajectory with control sequence $U^P = (\bar{u}[0], \bar{u}[1], \dots)$, if $(\bar{x}[k], \bar{u}[k]) \in (\mathbb{X} \times \mathbb{U})$, $\bar{x}[k] = \bar{x}[k+P]$, $\bar{u}[k] = \bar{u}[k+P]$ for all $k = 0, 1, \dots$. Then, $\Pi_U = (X^P, U^P)$ is called a periodic state-control sequence.

The distance measure

$$|(x[k], u[k])|_{\Pi_U} = \min_{(\bar{x}[i], \bar{u}[i]) \in \Pi_U} \|x[k] - \bar{x}[i]\| + \|u[k] - \bar{u}[i]\| \tag{23}$$

evaluates the Euclidean distance of a point $(x[k], u[k])$ to the closest state-control pair in the periodic state-control sequence.

If a system is strictly periodically dissipative w.r.t. a periodic sequence Π_U (see [3]), it will approach the corresponding trajectory and only (if necessary) leave it at the end of the horizon due to final constraints. This means it follows the periodic turnpike defined by Π_U.

Figure 3 shows the optimal solutions for three different periods of the exciting wave. The wave is assumed to be a sinusoidal disturbance $d(t)$ with appropriate amplitude such that energy can be extracted. In particular, we investigate the

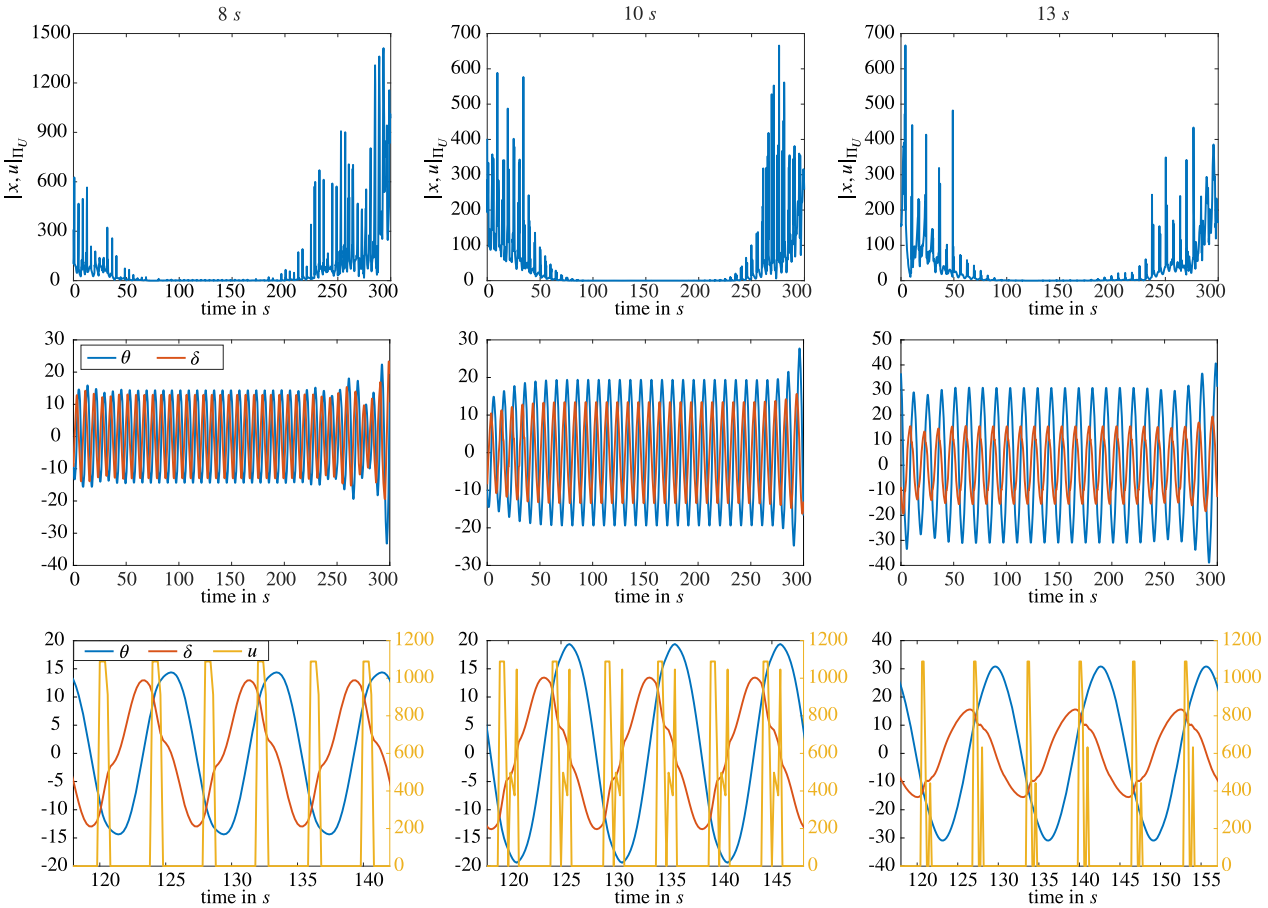

FIGURE 3 Optimal solutions are shown for three different wave periods. In all three cases, the system approaches a phase of periodic oscillations indicating periodic turnpike behavior.

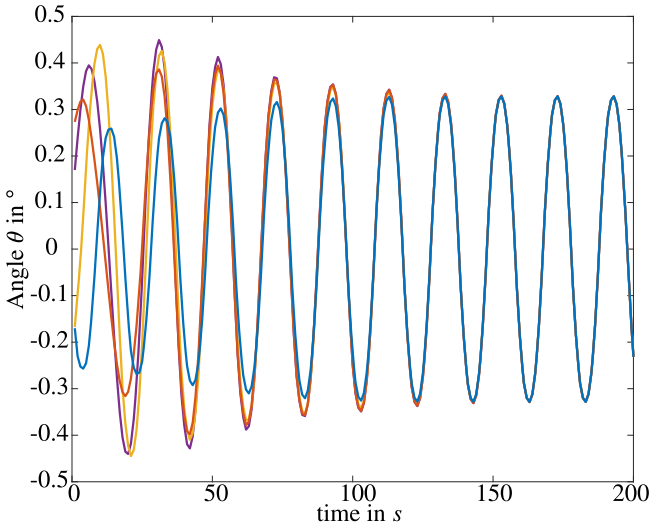

FIGURE 4 Four different initial conditions all end up in the same periodic trajectory, indicating again the periodic turnpike-behavior.

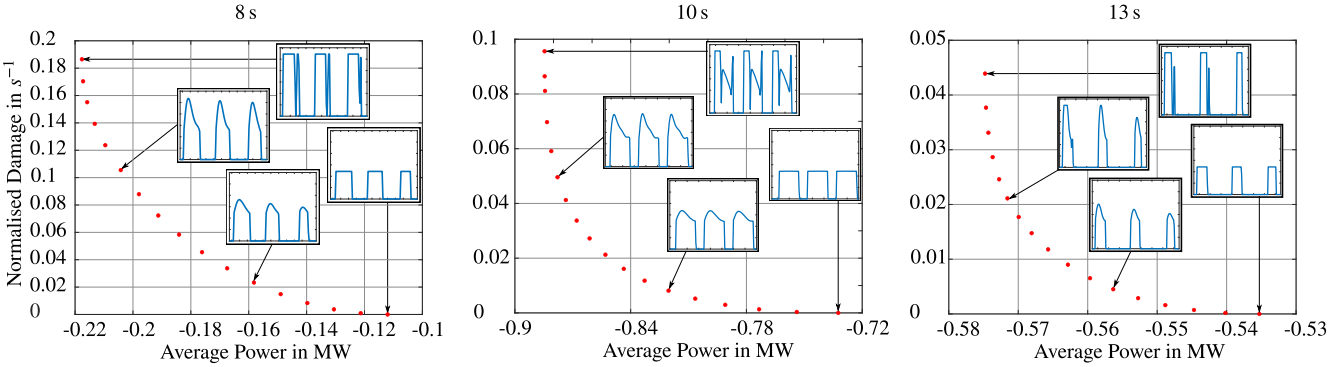

FIGURE 5 The Pareto fronts for actuation under harmonic excitation with different wave periods. In all three cases, there is a considerable trade-off between the energy and damage cost functions. Both are given as averages over the prediction horizon.

existence of turnpikes by applying the distance measure Π_U to the optimal state-control pair. In the first row of Figure 3, the distance measure Π_U decreases in the beginning, stays near zero in the middle part, and increases in the end. This corresponds to a periodic turnpike with incoming and leaving arcs. In the second row, one can see that the first two states, θ and δ, correspondingly approach and leave the turnpike phase of periodic oscillations. The third row shows a zoom into three periods of the oscillations during the middle part of the solution when the state and control signals should give a good approximation of the periodic turnpike trajectory.

The turnpike property of an optimal solution is known to hold independently of the initial point and the time horizon. To numerically check the former, we now solve Problem 1 for one fixed wave period but different initial conditions. The solutions are shown in a close-up in Figure 4: four different initial conditions lead to the same periodic trajectory.

All these observations still hold when the damage costs are taken into account as a second objective in a multi-criteria sense. In our previous work [16], we computed the Pareto fronts of Problem 1 to find the optimal compromises between J_1 and J_2, shown in Figure 5, where we found that there is a major trade-off between the harvested energy and the accumulated damage as it can be seen from the convexity of the Pareto front. Moreover, we concluded that energy can even be harvested when the voltage is low enough to not accumulate any damage within our model.

Let us now apply the distance measure Π_U , analogously to the study presented in Figure 3 for single-objective optimization. Figure 6 shows that even if major priority is put on the damage cost function, the optimal solution still approaches and stays on a periodic solution indicating a periodic turnpike.

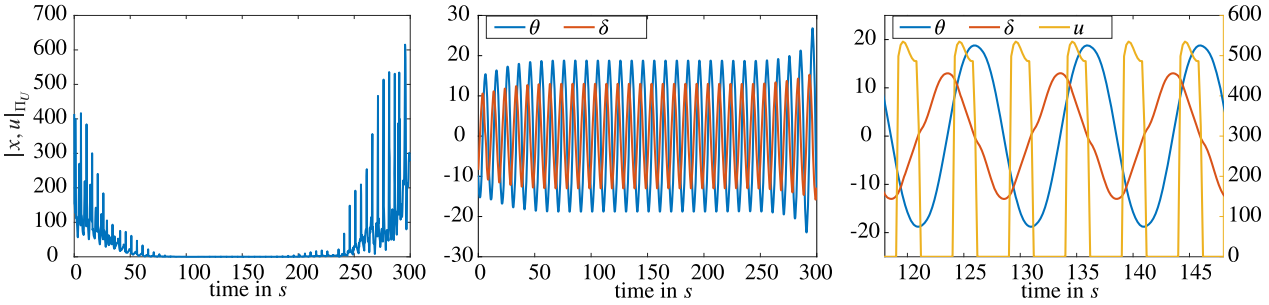

FIGURE 6 Even if the accumulated damage is considered as the second cost function in Problem 1, the periodic turnpike phenomenon still shows up for all exciting wave periods, here displayed for the example of 10 s. The solution shown was obtained using weighted sum scalarization with the weights [0.5 0.5].

4.1 | Concluding discussion

In Section 2, we showed the dissipativity of the DEG-WEC for the supply rate $s_{\text{WEC}}\ (x(t), u(t)) = \delta(t)d(t) - \gamma\delta(t)\theta(t)u(t)$, but motivated the cost function $J_1(x, u, t_0, t_1) = \int_{t_0}^{t_1} i(t)\sqrt{u(t)}\,\mathrm{d}t$, with the application of energy harvesting in mind. Minimizing $\int_{t_0}^{t_1} \delta(t)d(t)\,\mathrm{d}t$ means reducing the energy that the wave adds to the system, which is unwanted as this is the energy to be harvested. Still, we are able to show periodic turnpikes with this changed supply rate $s_{\text{pow}}\ (x(t), u(t)) = i(t)\sqrt{u(t)}$.

5 | MULTIOBJECTIVE MPC WITH STOCHASTIC WAVE EXCITATION

Recall that we have used a simple sinusoidal excitation so far. This is a poor model of wave dynamics, though. Thus, we give a more sophisticated model for generating stochastic wave excitation profiles in the following, for which we repeat the numerical MPC study. Moreover, we extend to multi-objective optimization (MOO)-MPC and discuss an automated decision making heuristic via weight selection. We derive MPC solutions for the previously considered monochromatic wave as well as for the stochastic case.

5.1 | Stochastic wave model

Stochastic waves can be approximated using a superposition of infinitely many sine waves that are scaled and shifted [18], resulting in the excitation

$$W_\infty(t) = \sum_{i=1}^{\infty} A_i \sin(\omega_i t + \phi_i(t))\,. \tag{24}$$

The amplitude scaling depends on the frequency ω_i of the sine wave and follows the Bretschneider spectrum, $S_{\text{B}}(\omega)$,

$$S_{\text{B}}(\omega) = A_{\text{B}}\omega^{-5}\exp\left(-B_{\text{B}}\omega^{-4}\right), \tag{25}$$

$$A_{\text{B}} = \frac{H_{\text{w}}^2}{4}\left(\frac{\omega_{\text{e}}}{2\pi}\Gamma\left(\frac{5}{4}\right)\right)^4, B_{\text{B}} = \left(\frac{\omega_{\text{e}}}{2\pi}\Gamma\left(\frac{5}{4}\right)\right)^4,$$

that describes amplitude scale distribution w.r.t. the frequency, with Γ as the gamma function. The coefficients A_{B} and B_{B} in Equation (25) are calculated using a dominant frequency ω_{e} and a significant wave height H_{w}. Frequencies close to the dominant frequency result in a higher scaling through the Bretschneider spectrum and the spectrum itself decays exponentially for $\omega \gg \omega_{\text{e}}$.

Since we cannot calculate the superposition of infinite sine waves, the spectrum will be approximated using a number of N_{w} sines with respective frequencies that are uniformly sampled from $\left[\frac{1}{3}\omega_{\text{e}},\ 3\omega_{\text{e}}\right]$. With a sufficiently high number of

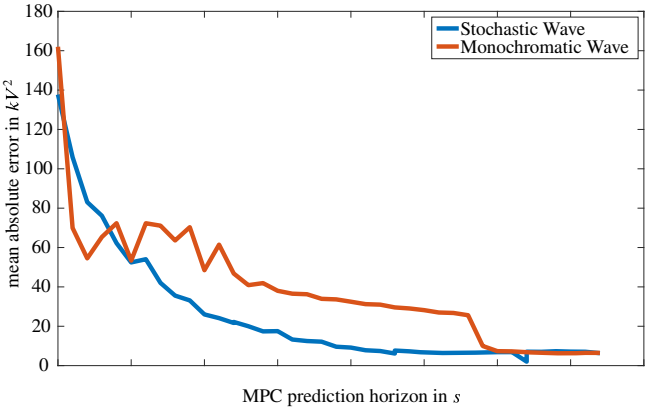

FIGURE 7 Comparison of MPC performance for monochromatic versus stochastic wave excitation. In both cases, ground truth is computed from an OCP on the long horizon. Depending on the MPC prediction horizon, monochromatic excitation (red) returns a smaller error than stochastic excitation (blue) or vice versa.

sine waves, Equation (25) can be rewritten and the ith amplitude, A_i expressed as

$$A_i = \sqrt{2S_{\mathrm{B}}(\omega_i)\Delta\omega_i}, \tag{26}$$

with ω_i being the ith angular frequency and $\Delta\omega$ the uniform sampling interval. The frequency shifts ϕ_i are initialized randomly and are typically constant over time. For a finite amount of sine waves the resulting wave $W_{N_{\mathrm{w}}}(t)$ would still repeat after some time. Numerically, this is significant enough to introduce a time-dependent phase shift $\phi_i(t)$. Starting from an initially randomized value $\phi_0^i \in [0,\ 2\pi]$ the phase shift changes slowly over time $\phi_i(t) = \phi_0^i + \phi_{\mathrm{f}}^i(t)$. To ensure the phase shift is continuous and does not change abruptly, a Fractional Brownian motion noise random number generator is used to calculate $\phi_{\mathrm{f}}^i(t)$. The change is so slow, that the effect is negligible for a small time horizon but still ensures no long-term periodicities arise. Lastly, the generated wave $W_{N_{\mathrm{w}}}(t)$ is multiplied with a frequency-dependent excitation coefficient (depending on the hydrodynamics) $\gamma_{\mathrm{F}}(\omega)$ to calculate the resulting excitation torque,

$$d(t) = \sum_{i=1}^{n_{\mathrm{f}}} \gamma_{\mathrm{F}}(\omega_i) A_i(\omega_i) \sin(\omega_i t + \phi_i(t)), \tag{27}$$

applied to the wave harvester flap.

5.2 | Performance analysis of the MPC

One interesting difference between monochromatic and stochastic waves is the performance of MPC. MPC is known to only approximate the optimal solution. We compare this approximation for the two types of excitation by varying the prediction horizon length of the MPC algorithm. Figure 7 shows the results generated by comparing the MPC with a ground truth OCP solution. For very short prediction horizons, the MPC performs equally badly for both types of waves. But while the performance steadily enhances for stochastic waves, the error stays high in the monochromatic case until it drops abruptly at one point. We suspect this behavior stems from the leaving arc projecting all the way to the part of the horizon that is applied to the system.

5.3 | Multiobjective MPC

As discussed above, at least the following two objectives are of interest for optimal operation of DEG-WEC: maximum energy harvesting and minimum system damage. This leads to an MOCP problem as introduced in Equation (22). Since the two objectives are conflicting, the multiobjective optimization provides a Pareto front of optimal compromises. In

the case of two conflicting and convex objective functions, the Pareto front is known to be a one-dimensional manifold. While in our case, only J_2 is convex, the Pareto front is, as previously shown in Section 4, convex and makes it reasonable to assume one connected component of the front without holes, dents, or kinks. Thus, for simplicity, we apply weighted sum scalarization, that is, we approximate the Pareto front by

$$\mathcal{P} = \left\{ \begin{pmatrix} J_1(x^*, u^*) \\ J_2(x^*, u^*) \end{pmatrix} \middle| \; (x^*, u^*) = \underset{x \in \mathbb{X}, u \in \mathbb{U}}{\arg\min} \, w_1 \cdot J_1(x, u) + w_2 \cdot J_2(x, u) \text{ w.r.t. dynamics(1) for } (w_1, w_2) \in \mathbb{W} \right\}.$$

Without loss of generality, let us assume increasing values of $w_{2,i}$ for increasing i.

5.4 | Automated decision making for multiobjective MPC

Decision making is required for choosing exactly one control signal for system operation in every MPC loop. To allow for an autonomously operating WEC system, automated decision making has to be provided.

In a previous study [15], we have shown that the Pareto fronts of a MOCP strongly depend on the wave excitation. Therefore, it is not advisable to a priori fix one set of weights $(w_{1,i}, w_{2,i})$. Instead, the decision making should automatically adapt to the current system state. Since we consider accumulated damage as our second objective in order to maximize the DEG-WEC lifetime, the decision making strategy can be borrowed from [25], in which active control of the residual useful lifetime via a selection of Pareto points for wind energy systems is presented. Let us assume we have to design optimal operational strategies not for a single WEC, but for an entire farm of WEC. Then, it is desirable to synchronize the expected lifetime of the individual WEC such that maintenance costs at sea are kept low. That is, minimizing the damage during WEC operation is of higher priority if a system has already accumulated a comparable high amount of damage. The other way around, if maintenance is scheduled in near future anyhow, a WEC in good status could be operated with priority put on maximal energy harvesting.

While a full implementation of a WEC farm optimal control is beyond the scope of this article, we do show the performance of our MOCP with a simplified threshold-based decision making (cf. also [15]): Let t_{bd} denote the target time for minimum lifetime, for example, defined by the maintenance interval. Then, the accumulated damage cost at time t_{bd} should not exceed a fixed value J^{d} (corresponding to a rupture threshold). Let us consider an initial weight index $i_{\text{w}} \in [1, n_{\text{w}}]$. To approximate the future damage accumulation we evaluate the MPC performance over N_p time steps into the past. The average rate of damage accumulation J_{ps} is estimated and the damage at the break-down time is predicted by assuming that the average damage accumulation trend continues as in the past N_p steps. If the predicted damage exceeds J^{d}, i_{w} is decreased by 1, meaning we give higher priority to minimizing damage and allow less energy harvesting. Otherwise, if the predicted damage falls below $c_{\text{d}} J^{\text{d}}$, with $c_{\text{d}} \in [0, 1]$, i_{w} is increased by 1. That is, we can safely harvest a larger amount of energy in the next steps. The heuristic is repeatedly evaluated every N_p steps, provided that the DEG was actuated with non-zero input during that time.

This defines a *weight control* block, which we include in the MPC loop, see Figure 8 for a schematic: Within the block, accumulated damage J_2 is evaluated on system states ξ in order to choose a current set of weights (w_1, w_2), such that the MPC block performs an ordinary single objective optimization which generates the current control signal u according to the environmental state defined by the wave excitation d.

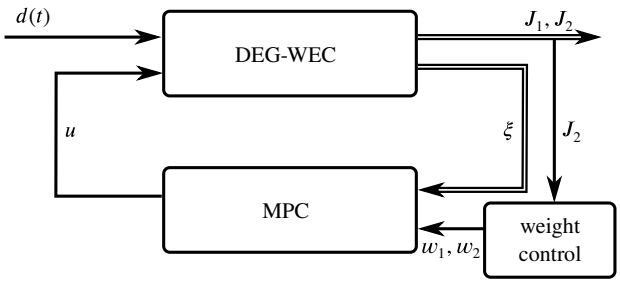

FIGURE 8 Schematic of the weight control which realizes an automated decision making within Pareto-optimal control strategies, based on the currently accumulated damage and the predicted increase.

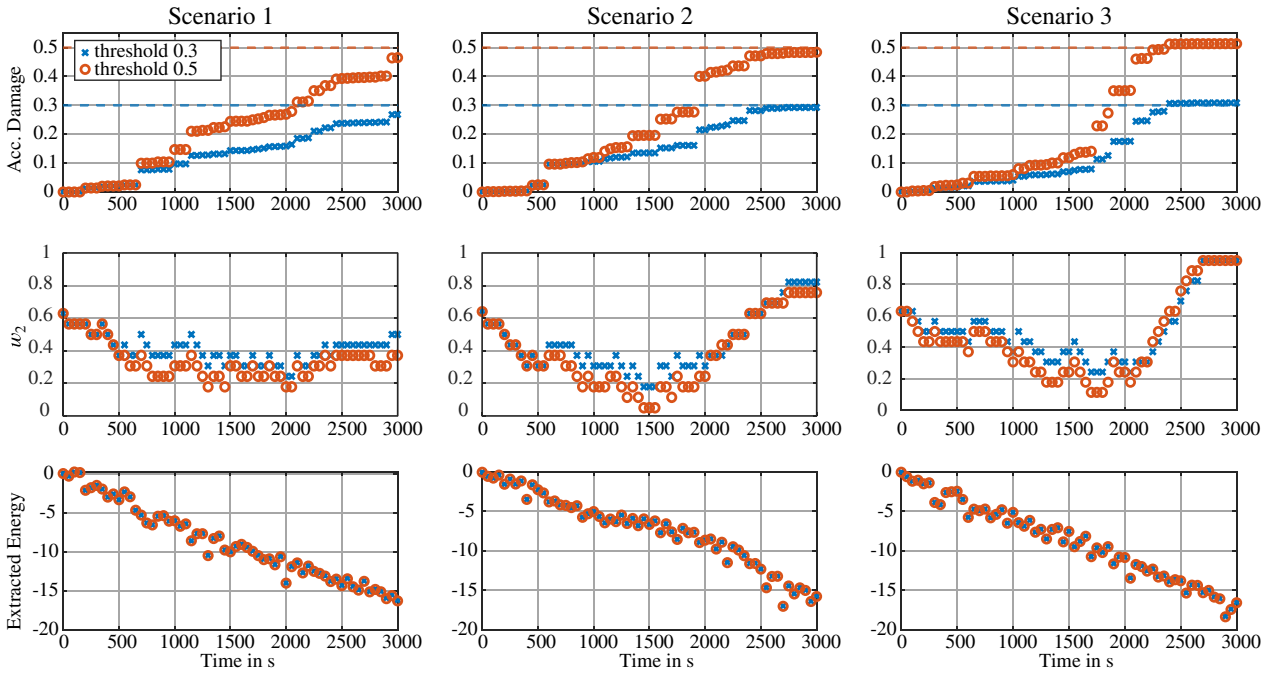

FIGURE 9 For three different stochastic wave scenarios, the weight controller is evaluated. For the first two scenarios, the controller approaches the target damage of 0.3 or 0.5, respectively. In the third scenario, the damage exceeds the target value, where it immediately increases the damage weight to the maximum of 0.95, resulting in a damage overshoot of less than 3%. The difference in the extracted energy is less than 6%.

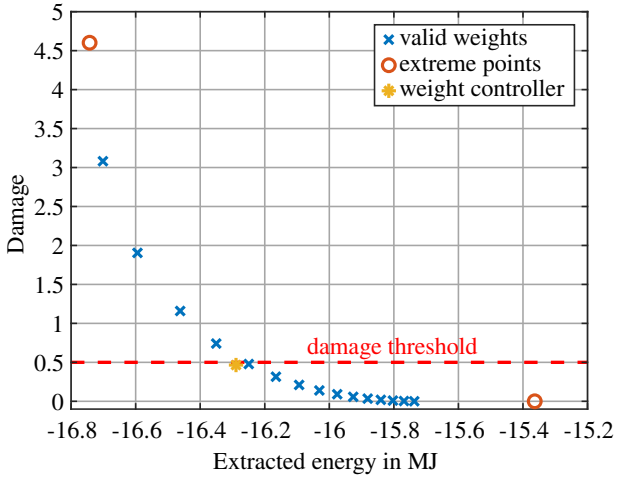

FIGURE 10 The weight controller with damage threshold 0.5 outperforms all of the fixed-weight MPC algorithms that satisfy the threshold, as it accumulates less damage while extracting more energy.

In Figure 9, the weight controller is compared to the MPC with fixed weights by simulating them for a simulation time of 3000 s and displaying their results in the objective space. Here, we use $n_w = 15$ equidistant weights for the weight controller and evaluate it in three different realizations of the same wave spectrum (i.e., the same hyperparameters, but different random values). Both scenario 1 and 2 approach their respective damage thresholds, while not overshooting and therefore potentially breaking the device. The lower damage is achieved by consistently keeping a lower energy-to-damage weighting. In the third scenario, the damage overshoots the target damage slightly by 3%, resulting in a quick adaption to maximum damage reduction. This ensures no further damaging to the device, without stopping the energy generation completely. In all cases, the difference in extracted energy between the higher and lower damage threshold is less than 6%.

Next, we compare the weight-controlled MPC with the MPC for fixed weights. The same weights as in the controller are used. Additionally, the MPC performance for approximate single objective solutions is calculated as extreme points by setting the weights close to $(0, 1)$ and $(1, 0)$, respectively. We observe in Figure 10 that the weight controller harvests more energy than all the fixed-weight counterparts that respect the damage threshold.

6 | CONCLUSION AND OUTLOOK

Wave energy harvesting by a dielectric elastomer flap-shaped generator proposes a challenging optimal control problem. Within this contribution, we present a control design approach that provided optimization-based receding horizon solutions. Thereby, stochastic wave excitation, assumed to be predictable on short time horizons, can be included in the model. Two objectives are of major importance: the amount of energy that can be harvested given the current wave excitation and the accumulated damage that eventually leads to system breakdown. Our numerical evaluations show that these objectives are conflicting and thus, lead to a Pareto front of optimal compromises. The chosen wave model is crucial for structural properties of the OCP and MPC: when considering a monochromatic sinusoidal excitation, we numerically show periodic turnpike behavior, even in the multiobjective case. An analytical study of strict dissipativity for periodic trajectories is up to future work. The MPC performs well also on a stochastic excitation model. Lastly, we introduce a rule-based decision heuristic for Pareto-points. This opens up interesting aspects of future research, for example, WEC farm control via more sophisticated rules for automated decision making in MOCP.

ACKNOWLEDGMENT

Open Access funding enabled and organized by Projekt DEAL.

FUNDING INFORMATION

GM received support from the European Union's Horizon 2020 research and innovation programme under the Marie Skłodowska-Curie grant agreement No 893674 (DEtune), and from the Italian Ministry of Education, University and Research (MUR) under the Program Department of Excellence, awarded to the Department of Industrial Engineering of the University of Trento, Italy.

REFERENCES

[1] F. B. Albuquerque and H. Shea, Influence of electric field, temperature, humidity, elastomer material, and encapsulation on the lifetime of dielectric elastomer actuators (DEAs) under DC actuation, Smart Mater. Struct. **30** (2021), no. 12, 125022.

[2] J. A. Andersson, J. Gillis, G. Horn, J. B. Rawlings, and M. Diehl, CasADi: A software framework for nonlinear optimization and optimal control, Math. Program. Comput. **11** (2019), no. 1, 1–36.

[3] J. Berberich, J. Köhler, F. Allgöwer, and M. A. Müller, Dissipativity properties in constrained optimal control: A computational approach, Automatica **114** (2020), 108840.

[4] Y. Chen, L. Agostini, M. Fontana, G. Moretti, and R. Vertechy. *On the lifetime performance of a styrenic rubber membrane for dielectric elastomer transducers*, ASME 2018 Conf. Smart Mater. Adapt. Struct. Intell. Syst., vol. 51944, American Society of Mechanical Engineers, V001T03A028.

[5] Y. Chen, L. Agostini, G. Moretti, G. Berselli, M. Fontana, and R. Vertechy, "*Fatigue life performances of silicone elastomer membranes for dielectric elastomer transducers: Preliminary results*," *Electroactive polymer actuators and devices (EAPAD) XXI*, Vol **1096616**, Y. Bar-Cohen and I. A. Anderson (eds.), International Society for Optics and Photonics, Bellingham, WA, 2019, pp. 27.

[6] R. G. Coe, G. Bacelli, H. Cho, and V. Nevarez. *A comparative study on wave prediction for WECs*, Tech Report, Sandia National Lab. (SNL-NM), Albuquerque, NM, 2018.

[7] I. Collins, M. Hossain, W. Dettmer, and I. Masters, Flexible membrane structures for wave energy harvesting: A review of the developments, materials and computational modelling approaches, Renew. Sust. Energ. Rev. **151** (2021), 111478.

[8] L. A. Dissado and J. C. Fothergill, *Electrical degradation and breakdown in polymers*, Vol **9**, Institution of Engineering and Technology, London, 1992.

[9] N. Faedo, S. Olaya, and J. V. Ringwood, Optimal control, MPC and MPC-like algorithms for wave energy systems: An overview, IFAC J. Syst. Control **1** (2017), 37–56.

[10] B. Geshkovski and E. Zuazua, Turnpike in optimal control of PDEs, ResNets, and beyond, Acta Numer. **31** (2022), 135–263.

[11] L. Grüne, Dissipativity and optimal control: Examining the turnpike phenomenon, IEEE Control. Syst. Mag. **42** (2022), no. 2, 74–87.

[12] L. Grüne, L. Krügel, and M. A. Müller, Multiobjective strict dissipativity via a weighted sum approach, Syst. Control Lett. **170** (2022), 105396.

[13] L. Grüne and M. A. Müller, On the relation between strict dissipativity and turnpike properties, Syst. Control Lett. **90** (2016), 45–53.
[14] L. Grüne and M. Stieler, Multiobjective model predictive control for stabilizing cost criteria, Discrete Continuous Dyn. Syst. B **24** (2018), 3905–3928.
[15] M. K. Hoffmann, L. Heib, G. Rizzello, G. Moretti, and K. Flaßkamp. Multi-objective model-predictive control for dielectric elastomer wave harvesters, 2022. https://doi.org/10.48550/ARXIV.2212.03511.
[16] M. K. Hoffmann, G. Moretti, G. Rizzello, and K. Flaßkamp, Multi-objective optimal control for energy extraction and lifetime maximisation in dielectric elastomer wave energy converters, IFAC-PapersOnLine **55** (2022), no. 20, 546–551.
[17] R. T. Marler and J. S. Arora, Survey of multi-objective optimization methods for engineering, Struct. Multidiscip. Optim. **26** (2004), no. 6, 369–395.
[18] G. Moretti. *Dielectric elastomer generators for wave energy conversion*, Ph.D. thesis, 2017.
[19] G. Moretti, M. Fontana, and R. Vertechy, Parallelogram-shaped dielectric elastomer generators: Analytical model and experimental validation, J. Intell. Mater. Syst. Struct. **26** (2015), no. 6, 740–751.
[20] G. Moretti, D. Forehand, R. Vertechy, M. Fontana, and D. Ingram. *Modeling of an oscillating wave surge converter with dielectric elastomer power take-off*, Int. Conf. Offshore Mech. Arct. Eng., vol. 45530, American Society of Mechanical Engineers, 2014, V09AT09A034.
[21] G. Moretti, M. S. Herran, D. Forehand, M. Alves, H. Jeffrey, R. Vertechy, and M. Fontana, Advances in the development of dielectric elastomer generators for wave energy conversion, Renew. Sust. Energ. Rev. **117** (2020), 109430.
[22] G. Moretti, S. Rosset, R. Vertechy, I. Anderson, and M. Fontana, A review of dielectric elastomer generator systems, Adv. Intell. Syst. **2** (2020), no. 10, 2000125.
[23] M. A. Müller, D. Angeli, and F. Allgöwer, On necessity and robustness of dissipativity in economic model predictive control, IEEE Trans. Autom. Control **60** (2014), no. 6, 1671–1676.
[24] A. Pecher and J. P. Kofoed, *Handbook of ocean wave energy*, Springer Nature, Cham, 2017.
[25] N. Requate, T. Meyer, and R. Hofmann, From wind conditions to operational strategy: Optimal planning of wind turbine damage progression over its lifetime, Wind Energy Sci. Discuss. (2022), 1–51.
[26] G. P. Rosati Papini, G. Moretti, R. Vertechy, and M. Fontana, Control of an oscillating water column wave energy converter based on dielectric elastomer generator, Nonlinear Dyn. **92** (2018), no. 2, 181–202.
[27] E. Trélat and E. Zuazua, The turnpike property in finite-dimensional nonlinear optimal control, J. Differ. Equ. **258** (2015), no. 1, 81–114. https://www.sciencedirect.com/science/article/pii/S0022039614003568.
[28] A. Wächter and L. T. Biegler, On the implementation of an interior-point filter line-search algorithm for large-scale nonlinear programming, Math. Program. **106** (2006), no. 1, 25–57.
[29] T. Whittaker and M. Folley, Nearshore oscillating wave surge converters and the development of oyster, Philos. Trans. R. Soc. A Math. Phys. Eng. Sci. **370** (2012), no. 1959, 345–364.
[30] J. C. Willems, Dissipative dynamical systems part I: General theory, Arch. Ration. Mech. Anal. **45** (1972), no. 5, 321–351.
[31] J. C. Willems, Dissipative dynamical systems part II: Linear systems with quadratic supply rates, Arch. Ration. Mech. Anal. **45** (1972), no. 5, 352–393.
[32] J. C. Willems and K. Takaba, Dissipativity and stability of interconnections, Int. J. Robust Nonlinear Control **17** (2007), no. 5-6, 563–586.
[33] Z. Yu and J. Falnes, State-space modelling of a vertical cylinder in heave, Appl. Ocean Res. **17** (1995), no. 5, 265–275.
[34] M. Zanon, L. Grüne, and M. Diehl, Periodic optimal control, dissipativity and MPC, IEEE Trans. Autom. Control **62** (2016), no. 6, 2943–2949.

How to cite this article: M. K. Hoffmann, L. Heib, G. Moretti, G. Rizzello, and K. Flaßkamp, *Optimal operation of dielectric elastomer wave energy converters under harmonic and stochastic excitation*, GAMM-Mitteilungen. (2023), e202300010. https://doi.org/10.1002/gamm.202300010